

## Absolute measurement of the optical polarizability of C<sub>60</sub>

A. Ballard, K. Bonin, and J. Louderback

*Department of Physics, Wake Forest University, Winston-Salem, North Carolina 27109*

(Received 8 May 2000; accepted 14 July 2000)

We report on a new optical technique that uses light forces and a time-of-flight spectrometer to make absolute measurements of cluster polarizabilities. This is also the first accurate report of an ac polarizability measurement of a condensable cluster in the gas phase. We have determined the optical polarizability of C<sub>60</sub> at the fundamental wavelength of a Nd:YAG laser (1.064 μm) to be  $\alpha = 79 \pm 4 \text{ \AA}^3$ . © 2000 American Institute of Physics. [S0021-9606(00)01038-2]

For the first time we report on a technique for measuring the ac polarizability of condensable clusters in the gas phase. As our first application, we have measured the polarizability of C<sub>60</sub> and the resulting measurement is the most accurate to date of a cluster larger than a dimer. Robust methods for accurately measuring electronic and optical properties are important to serve as benchmarks for theory since calculations of such properties for large, many-particle systems are challenging. In addition, our technique is important in four ways: (i) it provides an *absolute measurement* of the polarizability of clusters in the gas-phase, (ii) it is *universal*—the detection scheme is independent of the particular properties of the particle being measured, (iii) it can be extended to find *tensor polarizabilities*, and (iv) it could be applied to measure the *polarizability of ions* or ionic clusters. In this last way, our method is unique.

Until now, all gas-phase measurements of cluster polarizabilities have been in static fields. This includes metal clusters,<sup>1–4</sup> semiconductor clusters,<sup>5–7</sup> and insulating clusters.<sup>8,9</sup> For the first time, we report a direct measurement of the ac polarizability for a free cluster. Actually, an ac polarizability measurement of the C<sub>60</sub> cluster in the gas phase using Rayleigh scattering has been previously published,<sup>10</sup> but the reported value differs by a factor of 12 from our measured ac value, from the static value,<sup>8</sup> and from the mean of published theory values. Hence it is unclear what physical condition or experimental artifact their reported measurement represents. All previous cluster measurements have been relative measurements: for sodium and potassium clusters the atom was the reference;<sup>1</sup> for aluminum clusters, lithium atoms were the reference;<sup>2</sup> for semiconductor clusters the aluminum cluster measurements of de Heer<sup>2</sup> were the reference;<sup>5</sup> and for the lithium clusters (and lithium–sodium compounds) either lithium or sodium atoms were the reference.<sup>3,4</sup> For the static measurements of C<sub>60</sub> and KC<sub>60</sub>, lithium atoms were used. Note that the static-field deflection technique to measure cluster polarizabilities is not relative by nature, but it is more accurate to measure the cluster polarizability relative to an atomic “calibration standard” polarizability than to directly account for the electric-field pole geometry. An overview of polarizability physics (including that for clusters) can be found in Ref. 11, while a treatment of metal cluster physics can be found in the nice review by de Heer.<sup>12</sup>

Since this is the first report of this system in the literature, we will describe important aspects of the apparatus. There are three main experimental elements: a source for cold clusters, a cluster beam collimation tube that includes a light force interaction region, and a linear time-of-flight mass spectrometer—see Fig. 1. The cluster source is a dual-valve, front laser-vaporization source similar to that of Smalley and co-workers.<sup>13</sup> Helium gas is rapidly injected into a mixing chamber to cool the hot cluster plasma produced by laser-ablating a thin-film target of C<sub>60</sub>. This source produces significantly colder clusters than those produced by the single-valve, side laser-vaporization source we originally constructed. A unique feature of this source is that front ablation produces larger beam fluxes than side ablation sources. However, this geometry gives rise to the problem of bringing laser light down the vacuum-beam tube through a pair of collimating slits used to narrow the phase-space distribution of the cluster beam. Since the slits are narrow (slit gap=200 μm), light is severely diffracted when transmitted through the slits. As a result, we constructed a glass slit and a glass-metal slit to collimate our cluster beam *and* pass laser light. To our knowledge, this is the first report of the successful use of glass/glass-metal slits to collimate a particle beam.

The second element is the light force interaction region, consisting of a dielectric mirror mounted on the second slit assembly, but behind the second slit—see Fig. 2. A pulsed Nd:YAG laser beam ( $\lambda = 1.064 \text{ \mu m}$ ) is retroreflected off the mirror to produce a standing wave in a direction orthogonal to the cluster beam axis ( $z$ -axis). A cluster in an *oscillating field* that is detuned far from any resonances experiences a time-averaged force that is conservative. The conservative force only affects the motion along one dimension (the propagation axis of the laser,  $x$ -axis). The equation of motion for a molecule experiencing such a force can be written<sup>14</sup>

$$\frac{d^2x}{dt^2} = \frac{dv}{dt} = V(y,z)f(t)\sin(2kx), \quad (1)$$

where  $t$  is the time and  $k = 2\pi/\lambda$  is the wave vector of the light. The characteristic velocity  $V$  is

$$V(y,z) = \frac{16\pi^2}{M\lambda c} \mathcal{F}(y,z) \alpha_{zz}, \quad (2)$$

where  $M$  is the mass of the cluster,  $c$  is the speed of light, and

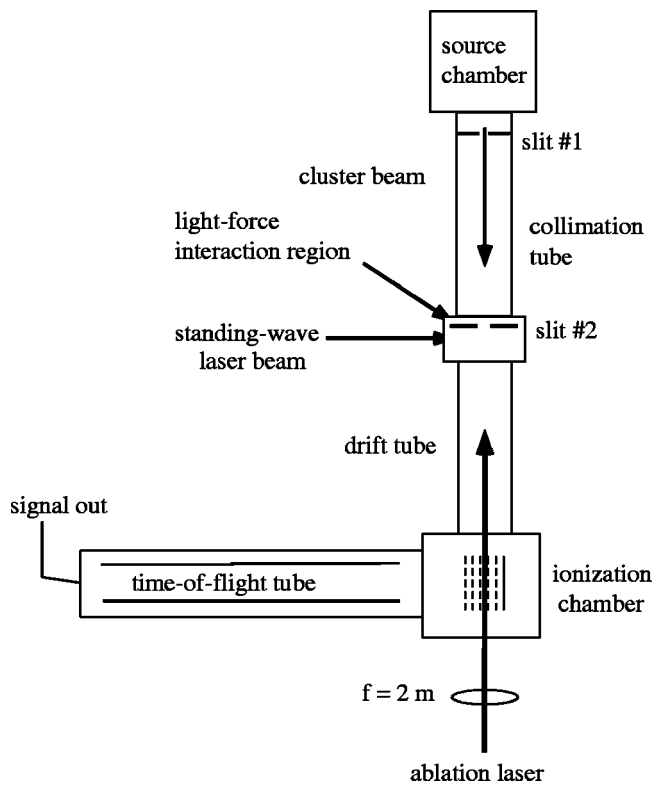


FIG. 1. A sketch of the experimental apparatus.

$$\mathcal{F}(y, z) = \frac{c}{8\pi} \int_{-\infty}^{\infty} E^2(y, z, t) dt \quad (3)$$

is the fluence (energy/area) of the laser pulse. Here  $E(y, z, t)$  is the electric-field vector length at position  $(y, z)$  at time  $t$ . In Eq. (1)  $f(t)$  is the slowly varying envelope of the laser pulse. Physically, the characteristic velocity corresponds to the maximum kick that can be given to a cluster by the light force. Here, the light is assumed to be linearly polarized along the  $z$ -axis. The polarizability in Eq. (2),  $\alpha_{zz}$ , corresponds to a particular component of the polarizability tensor (see Ref. 11). Since C<sub>60</sub> is isotropic, its polarizability  $\alpha$  is a scalar. The clusters experience a light force proportional to their polarizability at the laser frequency. The forces experi-

enced by the clusters interacting with the light are orthogonal to their motion and so they get deflected in both directions along the standing wave axis. The result is a redistribution of the clusters in phase space—see Fig. 2. The clusters receive velocity kicks whose magnitude depends on cluster position within the standing-wave beam. The Nd:YAG pulse is so short (it has a Gaussian temporal profile whose FWHM is  $\tau = 7$  ns) that each cluster stays nearly in the same position during the laser pulse. This assumption that the particles do not move a significant amount during the laser pulse is called the sudden impulse approximation. If, during the laser pulse, a particle moved over a significant region of space (say  $\lambda$ ), then the light force would average out and only a small net velocity kick would result. Extensive calculations<sup>14,15</sup> have shown that if each cluster moves less than  $\lambda/10$  during the laser pulse (arbitrarily chosen), then the sudden impulse approximation is excellent. For our experiment we estimate the motion during a pulse to be  $\lambda/20$ . The velocity kicks will, with the passage of time, manifest themselves as a spatial redistribution of the clusters in the direction orthogonal to the beam direction. This spatial redistribution occurs downstream of the light-force region. The theory of the light force, including a description of the phase space redistribution in some limiting cases, has been discussed earlier.<sup>14</sup> This reference and references therein<sup>15</sup> discuss in detail the applicability of the light-force interaction to the measurement of particle polarizabilities. Specifically, these references discuss the dependence of spatial and velocity distributions on light-force fluence, their dependence on detuning from resonances, how the laser pulse duration and laser polarization affect the interaction and distributions, and how the directions of the two intersecting light-force laser beams (to form a standing wave) affect the interaction.

The third experimental element is the ion chamber and linear time-of-flight mass spectrometer (TOFMS) that we built to separate and detect different cluster masses. The time-of-flight axis is perpendicular to the original cluster beam axis. Our TOFMS is a modified version of one designed by de Heer and co-workers.<sup>16</sup> We operate the TOFMS in a position-sensitive mode, where an ion's time-of-flight depends on its initial position at the time of ionization. The time-of-arrival curve produced by ions at the detector then corresponds to a spatial image of the clusters along the time-of-flight axis. This one-dimensional spatial distribution will change if the light force is applied, so the basic measurement consists of recording two different cluster ion versus time data sets. One set is the no light-force distribution and the other set is the light-force distribution. Clusters are ionized in the middle of the TOFMS acceleration plates ArF laser light at  $\lambda = 193$  Å. The light is focused with a fused quartz lens ( $f = 21$  cm at  $\lambda = 193$  Å). However, the clusters intersect the laser beam at a distance of  $f/3$  from the focal point. The estimated fluence of the ArF light in the ionization region is  $\phi \approx 20$  mJ/cm<sup>2</sup>. The ions were detected by an MCP array. The resulting signal was recorded by a fast digital oscilloscope and stored in files for later analysis. The experiment will be described in more detail in a longer paper.

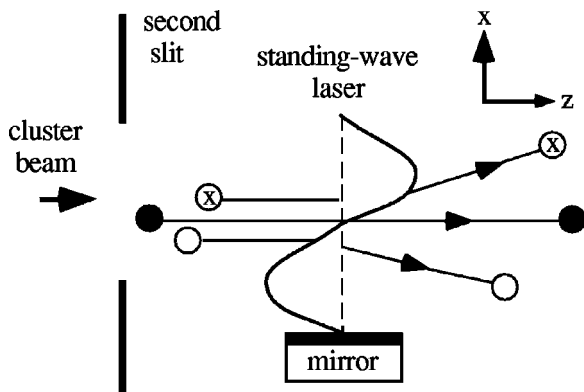


FIG. 2. Velocity kicks given to the clusters in the standing wave beam will change their downstream spatial distribution. The kicks are orthogonal to the original cluster beam direction.

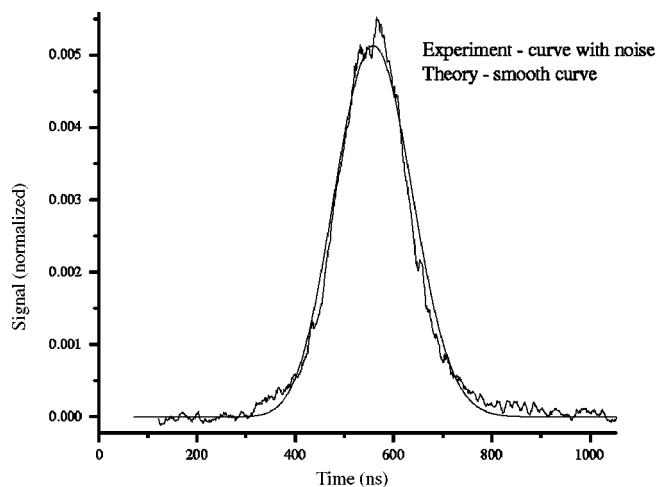


FIG. 3. Spatial distribution of  $C_{60}$  clusters when no light force is applied. The smooth curve is a theoretical fit to the experimental data.

To understand the data analysis needed to extract the polarizability, consider Fig. 3 which shows the number of cluster ions vs. time in the case of no light force. The cluster distribution consists of a group of  $C_{60}$  isotopes with the following probabilities: 720 amu—52.5%, 721 amu—34.1%, 722 amu—10.8%, 723 amu—2.20%, 724 amu—0.31%. In the position-sensitive mode, the TOFMS has its mass resolution significantly degraded from its peak, but it still retains the basic feature that different masses arrive at the detector at different times. However, the various  $C_{60}$  isotopes are not individually resolved in this mode, but are smeared out due to the inherent loss of time resolution in the position sensitive mode. This results in a  $C_{60}$  signal that is broadened compared to the case of only a single isotope. Hence the fitted curve in Fig. 3 represents the sum of five basic curves (one for each isotope) with weights that correspond to the probabilities of the different isotopes. The time that separates the curve for each isotope is determined from an ion optics program. We input our TOFMS plate geometry and the program calculates the mass dispersion ( $\Delta t/\Delta m$ ). The time-of-flight calculated with this program agrees to within 1.5% of our experimental observations. The resulting mass dispersion for our plate geometry and voltages is 42 ns/amu. This parameter is fixed in the fit to the experimental data. Also fixed in the fit is a broadening parameter  $\Gamma_{\text{laser}}$ , which accounts for the finite pulse length (FWHM=14 ns) of the excimer laser. Since ionization is a two-photon process here, we convolve the square of the temporally varying intensity of the excimer pulse with the basic cluster spatial distribution. In fact, the only parameters that are varied in generating the fit in Fig. 3 are the zero of time, i.e., the time shift of the fit relative to the experimental data and an additional broadening parameter which we label  $\Gamma_{\text{broad}}$ . We believe that the dominant contributor to  $\Gamma_{\text{broad}}$  is a broadening of the spatial distribution due to scatter of the clusters off of background gas in the vacuum. The vacuum in the region between the slits is  $5 \times 10^{-7}$  Torr with source off and about  $9 \times 10^{-7}$  Torr with source on. The vacuum in the TOFMS is  $3 \times 10^{-7}$  Torr. However, the total cluster path is about 3 m, which is quite long. Additional contributing effects to broadening are scat-

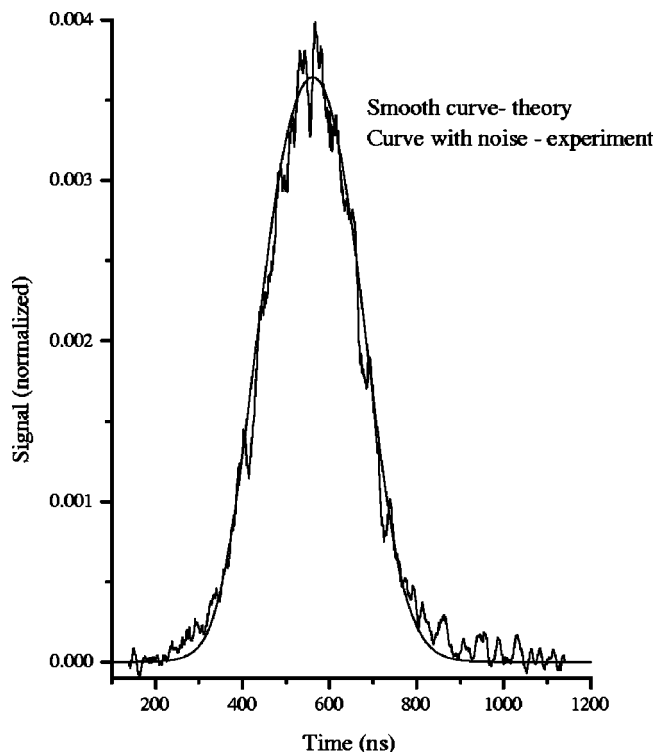


FIG. 4. Spatial distribution of  $C_{60}$  clusters when the light force is applied. The smooth curve is a fit to the experimental data.

ter off slit walls, perhaps a small amount of delayed ionization, and inhomogeneities in the fields in the TOFMS. To illustrate the size of the broadening parameter  $\Gamma_{\text{broad}}$  to the overall width, we note that the data in Fig. 3 exhibit a FWHM of  $\Gamma_{\text{FWHM}} = 160$  ns. The best fit gives  $\Gamma_{\text{broad}} = 70$  ns, and so the actual width in the absence of the  $\Gamma_{\text{broad}}$  broadening is  $\sqrt{\Gamma_{\text{FWHM}}^2 - \Gamma_{\text{broad}}^2} = 144$  ns. Hence, the  $\Gamma_{\text{broad}}$  broadening amounts to about a 10% effect.

To analyze the light-force data, consider Fig. 4. This is one of three curves that are simultaneously fit to determine the polarizability. When the light force is applied it is important to know which “slice” of the cluster beam is affected. Then, ideally, you would just ionize that slice of clusters. To understand these statements more clearly, note that the light-force laser beam (moving along the  $x$ -axis) is at right angles to the cluster beam (moving along the  $z$ -axis)—see Fig. 2. The length of the cluster beam along the  $z$ -axis is 14 cm (FWHM) while the intersecting YAG light-force laser beam has a width (along  $z$ ) of 7 mm. Hence the YAG will only affect a 7 mm “slice” of the cluster beam. We can decide which fraction of this 7 mm slice of the cluster beam to observe by adjusting the timing between the light-force laser and the ionization laser. Due to the structure on the light-force laser beam profile, different sections of the selected cluster beam “slice” are exposed to different laser fluences. To account for this, we measured the laser profile with a windowless CCD camera. We took three consecutive sets of data with different time intervals between the light-force laser pulse and ionization laser pulse. The precise difference in time between adjacent data sets was  $500 \pm 0.01$  ns. Since we know the speed of our clusters to better than 0.5%, we know

the spatial gap between the adjacent cluster slices. The three data curves that result are then fit to the theoretical curves using the fluence information from the camera. The fit parameters are the origin in time (time shift of theory curves relative to data curves) and the polarizability. The overall energy hitting the camera was measured using an energy meter. Since the size of a camera pixel is accurately known, the fluence on each pixel could then be calculated.

Our fits result in a C<sub>60</sub> polarizability value of  $\alpha = 79 \pm 4 \text{ \AA}^3$ . Several factors contribute to the error estimate. First, the calibration accuracy of the energy meter is 4%. Second, two fit parameters introduce error: the width  $\Gamma_{\text{broad}}$  from the no light-force data has an uncertainty of  $\pm 2.7\%$ ; the polarizability from the light-force data has an uncertainty of 2.1%. Finally, the uncertainty in the TOFMS for the isotope spacing is 1.5%. Combined in quadrature these uncertainties produce an overall error of 5%.

There has been a keen interest in the polarizability of C<sub>60</sub> due to the fact that this specie is at the crossroads between molecular and nanostructure science. As a result, a substantial variety of theoretical techniques, including condensed-matter methods, molecular structure calculations, and nuclear physics techniques, have been used to find values for the static C<sub>60</sub> polarizability. Although theoretical values for the static polarizability range from 36 to 154  $\text{\AA}^3$ , they average and cluster in the 80–85  $\text{\AA}^3$  range—see Ref. 11 for a summary. The static measurement in the gas phase is<sup>8</sup>  $76.5 \pm 8 \text{ \AA}^3$  and the thin-film results are in the 83–93  $\text{\AA}^3$  range—again see Ref. 11. Although no theoretical calculations for the dynamical polarizability of free C<sub>60</sub> have been published, it is relevant to discuss what frequency dependence we expect the polarizability to have. Perhaps the best guide for what to expect for the frequency dependence of  $\alpha$  comes from published measurements of the dielectric function  $\epsilon(\omega)$  for solid C<sub>60</sub>.<sup>17</sup> The frequency-dependent dielectric function was measured using UV-visible-IR reflection-transmission spectroscopy and ellipsometry. Here the polarizability is extracted from the dielectric function  $\epsilon(\omega)$  of solid fullerite films using the Clausius–Mossotti relation

$$\alpha(\omega) = \frac{3}{4\pi n} \left( \frac{\epsilon(\omega) - 1}{\epsilon(\omega) + 2} \right), \quad (4)$$

where  $n = 4/a^3$  is the number density of C<sub>60</sub> molecules in the face-centered cubic unit cell with a lattice constant  $a = 14.17 \text{ \AA}$ . The extracted polarizability  $\alpha(\omega)$  is plotted for  $\hbar\omega$  in the range 0–5 eV. The YAG wavelength ( $\lambda = 1.064 \text{ \mu m}$ ) corresponds to 1.16 eV. Their plot gives a calculated value for the C<sub>60</sub> polarizability at our YAG wavelength of  $\alpha(\hbar\omega = 1.16 \text{ eV}) \approx 82 \text{ \AA}^3$ . Interestingly, their plot of  $\alpha(\omega)$  for the thin film indicates that the C<sub>60</sub> polarizability drops slightly below its static value of  $\alpha(\hbar\omega = 0 \text{ eV}) \approx 83 \text{ \AA}^3$ —this is the electronic contribution only, an additional contribution of  $2 \text{ \AA}^3$  is due to the lattice. From their plot  $\alpha(\omega)$  reaches a minimum at  $\hbar\omega = 1.2 \text{ eV}$ . The depth of the dip is about  $2 \text{ \AA}^3$ . Obviously, the agreement between their thin-film value

and our value is quite good, although according to the relative values in their curve, our ac value should be slightly lower than the measured dc value. However, the measured static value for free C<sub>60</sub>, our measured ac value for free C<sub>60</sub>, and the values they extract from the dielectric function agree within error. We would expect  $\alpha(\omega) > \alpha(\text{dc})$  for the free C<sub>60</sub> cluster, since the main resonances for free C<sub>60</sub> begin in the blue at about 420 nm and the resonances grow stronger as  $\hbar\omega$  increases. The closest IR active vibronic resonances occur at about 0.15 eV, and they seem too far away and too weak to significantly affect the polarizability at 1.2 eV. Perhaps a theoretical calculation of free C<sub>60</sub> would show a slightly higher polarizability value at  $\lambda = 1.06 \text{ \mu m}$  than the dc value.

To summarize, we have developed a new technique for making absolute measurements of cluster polarizabilities. It is the first measurement of the ac polarizability of a condensable cluster in the gas phase and it is the most accurate measurement to date of the polarizability of a cluster larger than a dimer. We hope to apply it to other interesting clusters in the near future.

The authors are thankful for support from Wake Forest University and from the National Science Foundation (Contract No. 9420441). We thank Walt de Heer of Georgia Tech for many helpful discussions and Robert Haufler of Comstock, Inc. for his advice and suggestions about the cluster source. We are also grateful for drawings of the ablation source block from L-S. Wang of the University of Washington and for helpful discussions with Robert Compton of the University of Tennessee.

<sup>1</sup>W. D. Knight, K. Clemenger, W. de Heer, and W. A. Saunders, Phys. Rev. B **31**, 2539 (1985).

<sup>2</sup>W. de Heer, P. Milani, and A. Châtelain, Phys. Rev. Lett. **63**, 2834 (1989).

<sup>3</sup>E. Benichou *et al.*, Phys. Rev. A **59**, R1 (1999).

<sup>4</sup>R. Antonine *et al.*, J. Chem. Phys. **110**, 5568 (1999).

<sup>5</sup>R. Schafer, J. Woeckenhaus, J. Becker, and F. Hensel, Z. Naturforsch. **50a**, 445 (1994).

<sup>6</sup>S. Schlecht, R. Schafer, J. Woenckhaus, and J. Becker, Chem. Phys. Lett. **246**, 315 (1995).

<sup>7</sup>R. Schafer, S. Schlecht, J. Woenckhaus, and J. Becker, Phys. Rev. Lett. **76**, 471 (1996).

<sup>8</sup>R. Antoine, P. Dugourd, D. Rayane, E. Benichou, M. Broyer, F. Chandezon, and C. Guet, J. Chem. Phys. **110**, 9771 (1999).

<sup>9</sup>D. Rayane, R. Antoine, P. Dugourd, E. Benichou, A. Allouche, M. Aubert-Frecon, and M. Broyer, Phys. Rev. Lett. **84**, 1962 (2000).

<sup>10</sup>V. A. Maltsev, O. A. Nerushev, S. A. Novopashin, and B. A. Selivanov, Chem. Phys. Lett. **212**, 480 (1993).

<sup>11</sup>K. Bonin and V. Kresin, *Electric-Dipole Polarizabilities of Atoms, Molecules, and Clusters* (World Scientific, Singapore, 1997).

<sup>12</sup>W. de Heer, Rev. Mod. Phys. **65**, 611 (1993).

<sup>13</sup>R. Haufler, L-S. Wang, L. Chibante, J. Conceicao, Y. Chai, and R. Smalley, Chem. Phys. Lett. **179**, 449 (1991).

<sup>14</sup>M. A. Kadar-Kallen and K. D. Bonin, Phys. Rev. A **47**, 944 (1993).

<sup>15</sup>M. A. Kadar-Kallen, Ph. D. thesis, Princeton University (1992).

<sup>16</sup>W. de Heer and P. Milani, Rev. Sci. Instrum. **62**, 670 (1991).

<sup>17</sup>P. C. Eklund, A. M. Rao, Y. Wang, P. Zhou, K. A. Wang, J. M. Holden, M. S. Dresselhaus, and G. Dresselhaus, Thin Solid Films **257**, 211 (1995).